Articles

Elucidation of the Primary and Three-Dimensional Structure of the Uterotonic Polypeptide Kalata B1[†,‡]

Olav Saether,[§] David J. Craik,*[,∥] Iain D. Campbell,[⊥] Knut Sletten,[#] Jessie Juul,[#] and David G. Norman[○]

Department of Biochemistry, University of Oxford, South Parks Road, Oxford OX1 3QU, United Kingdom, Department of Biotechnology, SINTEF SI, PB 124, Blindern, N-0314 Oslo, Norway, Centre for Drug Design and Development, University of Queensland, St. Lucia, QLD 4072, Australia, Department of Biochemistry, Biotechnology Centre of Oslo, University of Oslo, PB 1125, Blindern, N-0317 Oslo, Norway, and Department of Biochemistry, The University, Dundee DD1 4HN, Scotland

Received September 6, 1994; Revised Manuscript Received December 16, 1994[⊗]

ABSTRACT: The amino acid sequence and structure of a uterotonic polypeptide extracted from the African plant *Oldenlandia affinis* DC have been determined. The peptide, kalata B1, consists of 29 amino acid residues and is rich in cysteine (6), threonine (5), and glycine (5). Enzyme cleavage studies show that the polypeptide backbone is cyclic. The three-dimensional solution structure has been determined using two-dimensional nuclear magnetic resonance (NMR) spectroscopy and distance-restrained simulated annealing. Kalata B1 is composed mainly of β-strands connected by tight turns, forming regions of β-sheet, except in the case of one section which forms a longer, less structured loop. The tertiary fold, together with the disulfides that form a sulfur core, produces a striking and unusual surface in which the majority of the hydrophobic residues form a solvent-exposed patch. The hydrophobic side of kalata B1 is flanked by two diametrically opposed and opposite-charged residues. The structure calculations have been used to predict the previously unknown disulfide bond connectivities using two approaches. In the first, a family of structures was calculated on the basis of NOE constraints without the assumption of a specific disulfide connectivity. The resultant structures were examined to determine whether the calculated position of the sulfur atoms suggested that one set of disulfide connectivities was more likely than the other, theoretically possible, sets. In the second approach, a separate family of structures (50 per set) was calculated for each of the 15 possible disulfide-bonded molecules. The resultant families of structures were compared to see whether one was favored over the others. Both approaches led to the same global fold, and the most likely disulfide connectivity is predicted to be 5−22, 13−27, and 17−29. In the calculated structure the cyclic peptide backbone is folded back onto itself and braced with disulfide pairs across diagonally opposed β-strands. This structure involves one of the disulfide bonds (5−22) threading through the eight amino acid loop formed by the other two disulfide bonds and the peptide fragments connecting them.

The tropical plant *Oldenlandia affinis* DC has long been used by African women for its action in accelerating contractions and childbirth. A native drug, *kalata-kalata*, is obtained by boiling the dried plant leaves to produce an extract which is sipped during labor (Gran, 1970). Initial chemical investigations showed that the plant leaves contain serotonin, a known uterotonic agent, and two polypeptides, kalata B1 and B2 (Gran, 1973a). The most abundant peptide species, kalata B1, has been isolated, partially characterized, and found to be uteroactive (Gran, 1973a). The second peptide-based component is present in significantly lower amounts and has not been characterized.

Kalata B1 consists of 29 amino acids, including six cysteines which are linked to form three disulfide bonds. In this paper it is shown that the main chain of the peptide is cyclic and that additional embedded cyclic loops are formed by the disulfides. The peptide is of interest because of its novel structure, its uterotonic activity, and the fact that it retains activity after several minutes of boiling. While the peptide is of limited clinical use as isolated because of unfavorable cardiac side effects (Gran, 1973b), it represents a starting point for the design of target-specific drugs acting on muscle. The development of such drugs will require detailed knowledge of the three-dimensional structure of the peptide, the impetus for this study.

The peptide is rather unusual in being cyclic and having three disulfide linkages in a relatively short amino acid sequence. As the connectivity of the disulfide linkages was not known, determination of this information from NMR data

[†] O.S. thanks the Norwegian Research Council for grant and financial support. The Oxford Centre for Molecular Sciences is supported by the MRC and SERC. D.J.C. thanks the Australian Department of Industry, Technology and Commerce for a travel grant.

[‡] Coordinates have been deposited with the Brookhaven Protein Data Bank under the file name 1KAL.

* Author to whom correspondence should be sent: telephone, 61-7-365 4945; Fax, 61-7-365 2487; Email, David@vcp.monash.edu.au.

[§] SINTEF SI.

[∥] University of Queensland.

[⊥] University of Oxford.

[#] University of Oslo.

[○] The University of Dundee.

[⊗] Abstract published in *Advance ACS Abstracts,* February 15, 1995.

0006-2960/95/0434-4147$09.00/0

alone was a challenge. Several determinations of the structure of small (<50 amino acids), multiply disulfide-linked proteins have been reported, in some cases (Holak et al., 1989) with prior chemical knowledge of the disulfide pattern and in others (Saudek et al., 1991; Cooke et al., 1992; Johnson & Sugg, 1992) without this information. In principle, a combination of local and global analysis of NMR data can be used to derive disulfide bonding patterns (Klaus et al., 1993). The objective of the current study was to determine the three-dimensional structure of kalata B1 together with a prediction of the disulfide bond connectivity.

To address the problem of the lack of disulfide connectivity information, two approaches were used. One involved the calculation of a family of structures based on the NOE data but in which no explicit linking of cysteines was applied. Distances between pairs of sulfur atoms were examined to determine which of the 15 possible bonding patterns was most probable in the derived structures. The second approach involved calculation of families of structures representing all 15 possible disulfide bonding patterns (i.e., with the cysteines explicitly bonded), followed by analysis of potential energies, restraint violations, and various geometrical parameters.

MATERIALS AND METHODS

The purity of kalata B1 was checked by analytical high-performance column chromatography (HPLC) (Sletten et al., 1981) and high-performance capillary electrophoresis (CE). The CE was performed in a 50 cm × 75 μm fused silica cartridge (Beckman, P/ACE System 2000) with a 50 mM sodium phosphate buffer at pH 2.5, constant voltage of 20 kV, and constant temperature of 30 °C. The detector was set at 214 nm. The molecular mass of the peptide was determined using ion-spray mass spectrometry (VG Bio-Q). Amino acid composition was determined after acid hydrolysis for 24 h at 110 °C using an automated amino acid analyzer (Biotronik LC 5000). The cysteine content was determined as cysteic acid from performic acid oxidized samples (Hirs, 1956). In addition, independent values were obtained from reduced and alkylated kalata using previously described methods (Sletten et al., 1981).

Automatic Edman degradation was carried out in a 477A protein sequencer (Applied Biosystems). The PTH amino acid derivatives were determined on-line with an Applied Biosystems 120 PTH analyzer. Some of the N-terminal analyses were performed in a Jeol 47 K spinning-cup sequencer (Sletten et al., 1981). In these cases, derivatives were analyzed by gas chromatography (GC) and thin-layer chromatography (TLC). The polypeptide was cleaved with BNPS-skatole (Fontana, 1972) with hydroxylamine (Bornstein, 1970) and dilute acid. Reduced and alkylated kalata B1 was digested with trypsin and the protease *Staphylococcus aureus* V8 (Austen & Smith, 1976). The peptides derived were purified by TLC and HPLC as previously described (Sletten et al., 1981).

NMR Spectroscopy. NMR spectra were recorded on a Bruker AM 600 spectrometer. All two-dimensional (2D) spectra were recorded in the pure phase absorption mode using time-proportional phase incrementation (TPPI) (Redfield & Kuntz, 1975; Bodenhausen et al., 1980; Marion & Wüthrich, 1983).

NOESY (Jeener et al., 1979; Macura et al., 1981) spectra were recorded at 303 and 323 K in D_2O and 90% H_2O/10% D_2O with mixing times of 60, 100, and 200 ms. Zero-quantum coherence effects were suppressed with a 5% random variation of the mixing time. For measurements in H_2O, the water resonance was suppressed by a semiselective "jump and return" sequence ($90°_x-\tau-90°_x$) (Plateau & Gueron, 1982) in place of the last 90° pulse of the NOESY sequence. A τ value of 90 μs was used with a 7000-Hz spectral width. Optimization of the receiver phase was performed to eliminate baseline distortions (Marion & Bax, 1988). Typically, 800−1024 increments of 2K data points were collected per experiment, yielding, after zero-filling, spectra with digital resolution of the order of 6−8 Hz/point in each dimension. In spectra used for assignment purposes, Lorentz-to-Gaussian convolution was applied in F_2 and a $\pi/5$ phase-shifted sine-squared bell window function in F_1. For 2D spectra, in which cross-peaks were integrated to obtain distance constraints, mild window functions ($\pi/2$ shifted sine bell) were used in both dimensions. Double-quantum-filled (DQF) COSY spectra (Rance et al., 1983) were also recorded in D_2O and H_2O at 303 and 323 K. Suppression of the solvent resonance was achieved by selective irradiation during the relaxation delay. A $\pi/8$ phase-shifted sine-bell window function was utilized for data processing in both dimensions.

HOHAHA (Braunschweiler & Ernst, 1983; Davis & Bax, 1985; Bax & Davis, 1985) spectra were recorded at 303 and 323 K. The radio-frequency (RF) pulses were generated via the high-power decoupler channel (90° pulse, ~25 μs) with a WALTZ-17 spin lock sequence (Bax, 1988); 1.5-ms "trim" pulses bracketed the WALTZ-17 sequence. Total mixing times used were 55 and 80 ms.

Structure Calculations. Structure calculations were performed with the program X-PLOR (Brünger, 1992) using two computational methods.

(a) Simulated Annealing. Starting structures were created by a two-step protocol. The first step was the generation of linear peptides within random ϕ and ψ angles. In the second, the peptides were cyclized by simulated annealing (Nilges et al., 1988; Nilges, 1990) followed by conjugate gradient minimization using a single distance restraint in place of the missing peptide bond. In cases where disulfide bonds were included, they were explicitly formed just prior to the cooling stage. An extra final step of the refinement was 200 steps of conjugate gradient minimization using a CHARMM (Brooks et al., 1983) force field with the dielectric constant set to 80 and the distance restraint potential set to 10 kcal mol^{-1} A^{-2}. Twenty structures were calculated for each of the disulfide families.

(b) Hybrid Distance Geometry/Simulated Annealing. Because of the unique cyclic and highly constrained nature of this peptide, it was important to ensure that structures were not biased by the computational method used. A second series of structures was therefore calculated using a hybrid distance geometry/simulated annealing method. The distance geometry phase of the protocol involved a sub-embed of backbone and a subset of β side-chain atoms, followed by fitting of the remaining atoms onto the sub-embed template as documented in the X-PLOR manual (Brünger, 1992). The structure was subsequently refined by simulated annealing. A fundamental difference between this and the previous method is that no manual cyclization step was required to generate suitable starting structures for the simulated annealing. Fifty structures were calculated for each of the

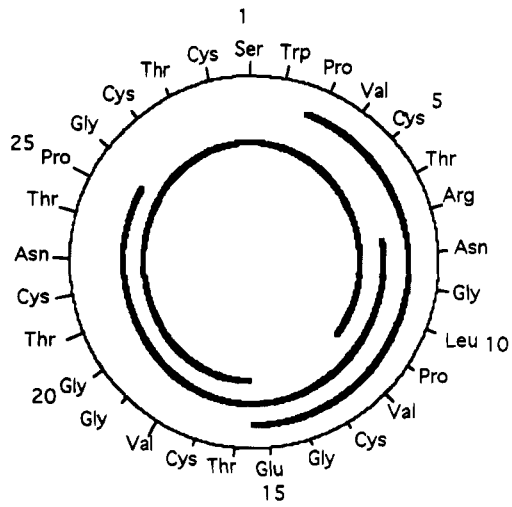

FIGURE 1: Primary structure of kalata B1 with inner arcs representing digest fragments from which sequence information was obtained.

disulfide families and for the case where no disulfide bonds were included.

RESULTS

The isolation and purification of kalata had been previously described (Gran, 1973a,b), but its sequence, disulfide connectivity, and structure were unknown. In the current study, its amino acid sequence was determined by chemical sequencing of partially overlapping fragments and its molecular mass by ion-spray mass spectrometry. From these experiments, it became apparent that the peptide is cyclic (i.e., possesses no free C- or N-termini, as they are connected via an amide bond) and, in addition, incorporates three disulfide linkages. The peptide comprises 29 amino acid residues which are arbitrarily numbered, starting from the single serine residue in the sequence as shown in Figure 1.

Primary Sequence Determination and Evidence for Cyclic Structure. The purity of kalata B1 was checked by HPLC and CE, revealing a single symmetrical peak in both systems. Molecular mass analysis indicated one molecule species of 2892 Da. Amino acid analysis of the native peptide, as well as of the oxidized or cysteine alkylated peptide, revealed no free N-terminus. Cleavage of the performic acid-oxidized peptide with BNPS-skatole followed by N-terminal analysis indicated a free N-terminal residue, resulting in the elucidation of positions 3−15, as indicated in Figure 1. From a digest of carboxymethylated kalata B1 with the protease *Staphylococcus aureus* V8, a peptide was purified which, with Edman degradation for 25 cycles, revealed the amino acid sequence of positions 16−29, continuing to serine at position 1 and overlapping with the BNPS-skatole-derived peptide until position 11 (Figure 1). From a tryptic digest of the S-methylated kalata B1, the amino acid sequence of positions 8−17 was determined. Several other peptides covering positions 1−5, 6−7, 8−13, 18−22, 9−21, 2−7, 9−15, and 20−22 were determined by Edman degradation. The amino acid sequences of these fragments confirmed the established data from the earlier digests. The combined data unambiguously confirmed the cyclic nature of kalata B1.

The amino acid sequence data are in agreement with the amino acid composition reported earlier (Gran, 1973a,b). The calculated molecular mass for the cyclic sequence shown in

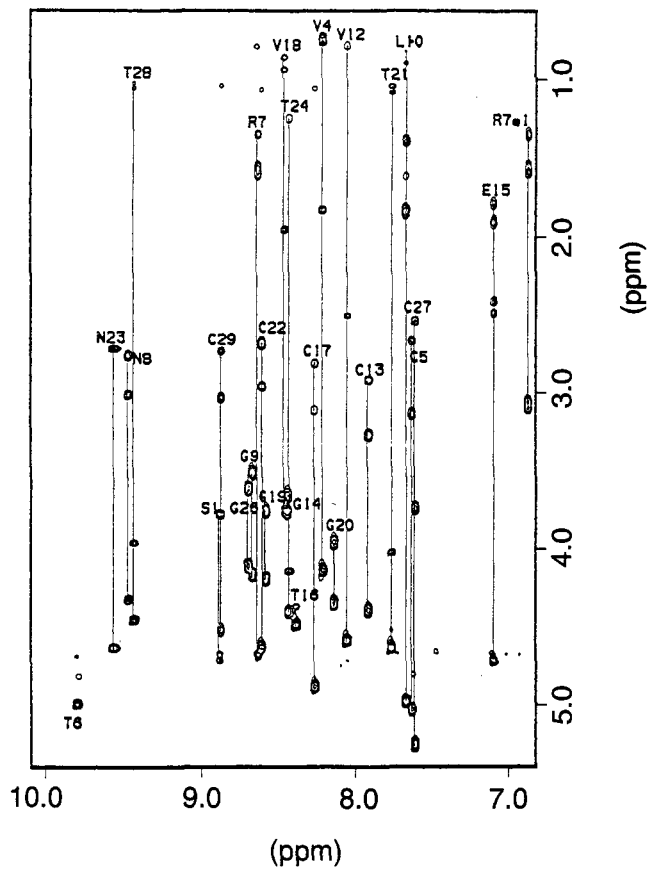

FIGURE 2: HOHAHA spectrum in H_2O of kalata B1 (pH 3.3, mixing time 55 ms, temperature 303 K) showing assignments of side-chain spin systems linked with their corresponding amide protons. The vertical lines connect peaks belonging to the same spin system (amino acid). Sequential identities are indicated next to the lines.

Figure 1, assuming three disulfide bridges, 2892 Da, agrees with that found by mass spectrometry.

The amino acid sequencing gave no information about the pairings of the disulfide bridges. Thus, one of the aims of the present study was to determine whether this information could be obtained from NMR data. It was anticipated that a knowledge of the 3D structure would be of considerable assistance in understanding receptor-binding interactions of kalata and, potentially, its biological activity.

NMR Assignments. In the 1D spectrum of kalata in 90% H_2O/10% D_2O at 303 K, the chemical shifts are well dispersed, suggesting the possibility of a well-defined structure. Before the structure could be determined, however, it was necessary to assign peaks in the spectrum to individual protons and to determine distance constraints between them. This was done using a combination of DQF-COSY, HOHAHA, and NOESY 2D NMR spectra.

The sequence comprises 10 AMX spin systems, five glycine AX systems, and five threonine spin systems, as well as three prolines, three valines, and single instances of leucine, glutamic acid, and arginine. Of the 10 AMX spin systems, nine are identified in the HOHAHA spectrum, shown in Figure 2, which traces connectivities from the NH proton to the α and β protons of each spin system. The missing AMX pattern, which was subsequently found to be due to W2, was located in the NOESY spectrum where cross-peaks from the only aromatic spin system in kalata to the β-methylene protons were detected. The W2 residue was

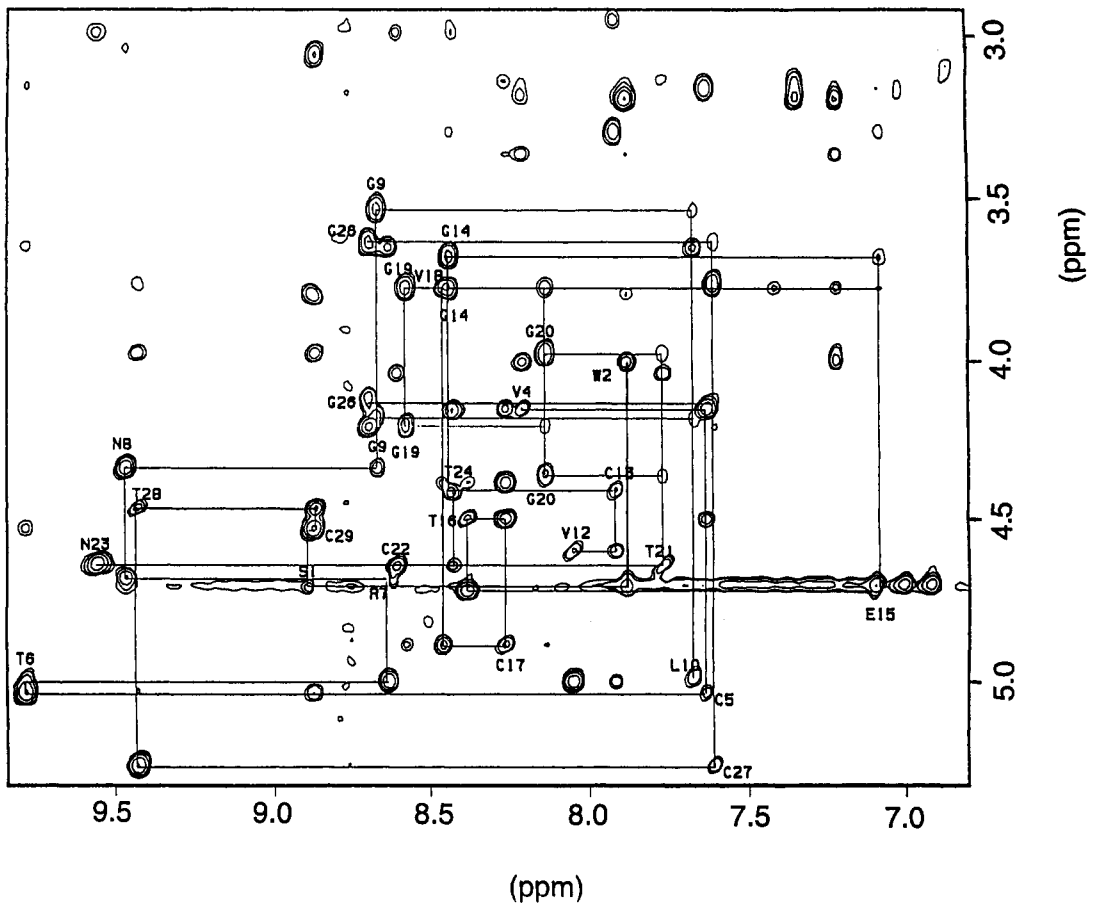

FIGURE 3: NOESY spectrum of kalata B1 in 90% H_2O/10% D_2O (pH 3.3, mixing time 200 ms, temperature 303 K) showing sequential assignments in the fingerprint region. The lines connect αH and NH protons in neighboring residues. The following sequences are traced: 4−10, 12−24, and 26−2. The trace is only broken at proline residues.

also the only one not to yield the expected NH−αH cross-peak in the fingerprint region of the DQF-COSY spectrum. This, and the lack of cross-peaks in HOHAHA spectra, was subsequently found to be consistent with the derived structure, as this residue is in a β-turn and is expected to have a small NH−αH coupling constant.

Of the other nine AMX spin systems, that with an NH chemical shift of 8.80 ppm was assigned to the single serine in the molecule, based on the characteristic low-field shift of the β protons, which are degenerate in this case. The remaining eight AMX systems comprised six cysteine and two asparagine residues. The latter were distinguished on the basis of characteristic NOE connectivities between the side-chain amide group and the corresponding β and/or α protons of the same residue.

The glycine residues were readily identified by their characteristic multiplet structure for cross-peaks between the amide backbone NH and the two α protons in the DQF-COSY spectra. Each of the five glycine residues shows separate resonances for the individual α protons in both DQF-COSY and HOHAHA spectra, the chemical shift differences for the pairs ranging from 0.1 ppm for G14 to 0.65 ppm for G9.

The five threonine residues yielded cross-peaks in a characteristic region of the DQF-COSY spectra, thereby identifying the methyl and β shifts of the spin systems. For several of the threonine residues, there were ambiguities in the DQF-COSY spectra in tracing connections back from the β to the α protons. In some cases, these ambiguities were resolved by reference to the HOHAHA spectrum (Figure 2); however, in a number of instances the HOHAHA spectrum did not display the full spin systems for the threonine residues. NOESY spectra were used to resolve any remaining ambiguities.

The proline residues were assigned on the basis of DQF-COSY and HOHAHA spectra. Signal overlap of some proline resonances and those of adjacent residues made it difficult to unambiguously determine the proline amide bond geometries in all cases. In the structure calculations described later the bonds were thus arbitrarily set as *trans*, although the possibility of one or more being in the *cis* form cannot be excluded.

The three valine residues were relatively easy to assign on the basis of their characteristic patterns in the DQF-COSY spectra. The γ-methyl shifts were nondegenerate for each valine residue.

The remaining residues occurred only once in the sequence and presented no difficulty in their assignment. They provided useful markers for the sequential assignment of the multiply occurring residues.

Having established the assignment of cross-peaks to residue type, the sequential assignment process was carried out as represented in Figure 3. This shows the fingerprint region of a 200-ms NOESY spectrum of kalata recorded in 90% H_2O/10% D_2O solution. In this, the connections between the α proton of one residue and the NH proton of the sequentially following residue are traced in an unbroken chain, apart from the three proline residues, which have no

Table 1: Chemical Shifts[a] of Kalata B1 (ppm) in H_2O at 303 K

position	residue	NH	Hα	Hβ	other
1	Ser	8.90	4.72	3.80, 3.80	
2	Trp	7.90	4.02	3.20, 3.20	2H 7.24; 4H 7.36; 5H 7.04; 6H 7.14; 7H 7.44; NH 10.35
3	Pro		3.37	1.65, −0.25	CH_2 1.20, 1.24; CH_2 3.19, 3.19
4	Val	8.23	4.15	1.85	γCH_3 0.80, 0.75
5	Cys	7.67	5.07	3.16, 2.69	
6	Thr	9.81	5.01	3.70	γCH_3 0.82
7	Arg	8.66	4.70	1.63, 1.60	γCH_2 1.37, 1.37; ϵCH_2 3.13, 3.08
8	Asn	9.49	4.34	3.03, 2.78	NH_2 7.52, 6.88
9	Gly	8.70	4.19, 3.54		
10	Leu	7.70	4.98	1.88, 1.42	γH 1.65; δCH_3 0.92, 0.86
11	Pro		5.02	2.40, 1.65	CH_2 2.18, 2.04; CH_2 3.66, 3.66
12	Val	8.08	4.60	2.53	γCH_3 0.82, 0.73
13	Cys	7.96	4.43	3.29, 2.94	
14	Gly	8.45	3.78, 3.68		
15	Glu	7.10	4.73	1.94, 1.81	CH_2 2.52, 2.45
16	Thr	8.40	4.51	4.40	γCH_3 1.10
17	Cys	8.29	4.90	3.12, 2.84	
18	Val	8.48	3.78	1.92	γCH_3 0.97, 0.89
19	Gly	8.60	4.22, 3.78		
20	Gly	8.16	4.37, 3.98		
21	Thr	7.80	4.65	4.04	γCH_3 1.10
22	Cys	8.63	4.65	2.98, 2.70	
23	Asn	9.58	4.65	2.76, 2.76	NH_2 7.60, 6.84
24	Thr	8.45	4.43	4.15	γCH_3 1.07
25	Pro		4.21	2.27, 1.84	CH_2 1.82, 2.02; CH_2 4.10, 3.66
26	Gly	8.72	4.12, 3.64		
27	Cys	7.64	5.27	3.77, 2.57	
28	Thr	9.44	4.47	3.98	γCH_3 1.08
29	Cys	8.91	4.53	3.05, 2.75	

[a] Chemical shift measured relative to H_2O at 4.72 ppm.

NH proton. Additional sequential connections between neighboring amide protons are summarized in Figure 4, and a complete assignment of chemical shifts is in Table 1. $^3J_{HN\alpha}$ values for the backbone were obtained from DQF-COSY spectra, and their magnitudes are given in Figure 4.

The rate of exchange of amide protons with deuterons from the solvent was determined qualitatively by monitoring the disappearance of amide proton peaks from 2D spectra. This was done for a sample freeze-dried from H_2O and dissolved in D_2O immediately prior to recording several 2D spectra. Amide protons detected in a NOESY spectrum recorded over 24 h, starting 0.5 h after dissolution of the sample in D_2O, were classified as slowly exchanging and are indicated in Figure 4. This information was subsequently used, in conjunction with structure calculations based on NOE's, to identify possible hydrogen bonding interactions. The spectra of, partially, amide-exchanged kalata B1 were also useful for the confirmation of some assignments due to the reduced number of overlapping amide resonances observed. In particular, the amide proton chemical shifts of S1 and C29 coincide; however, at 303 K, the S1 NH proton is slowly exchanging whereas the NH proton of C29 rapidly exchanges. In a partially exchanged sample of the peptide, NOESY cross-peaks could be observed between the S1 amide proton and both β protons of C29.

Analysis of Secondary Structure. In addition to the sequential NOE's indicated in Figure 4, kalata B1 exhibits

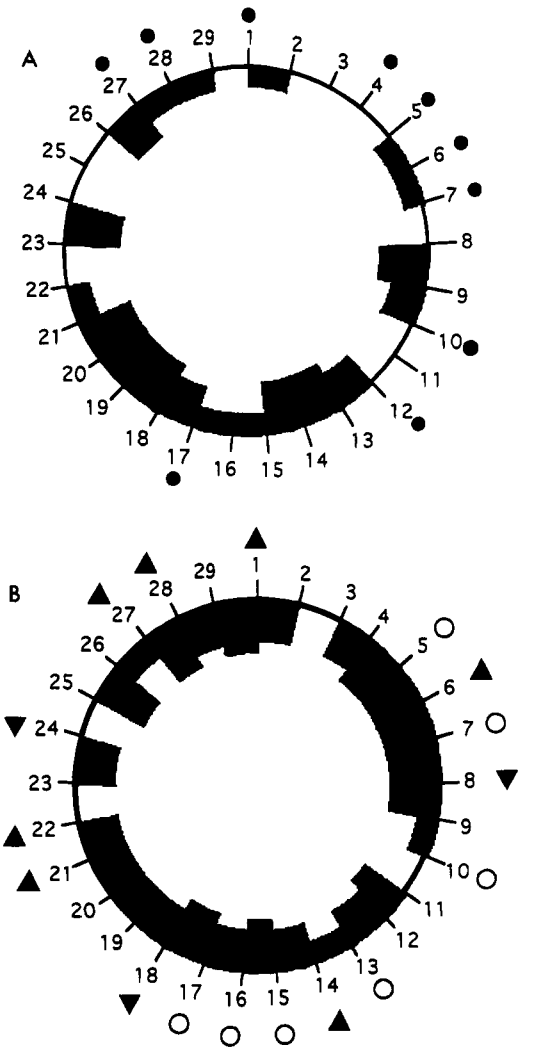

FIGURE 4: Summary of experimental data used to identify secondary structure in kalata B1. Black boxes represent NOE's (the size of the box relates to the size of the NOE). (A) shows $d_{N,N}(i,i+1)$ NOE's and (B) shows $d_{\alpha N}(i,i+1)$ NOE's. Black circles indicate the positions of slowly exchanging backbone amide protons; up-pointing triangles indicate $^3J_{HN\alpha}$ coupling constants greater than 8 Hz; down-pointing triangles represent $^3J_{HN\alpha}$ coupling constants less than 6 Hz; open circles indicate values in the range 6−8 Hz.

a substantial number of medium- and long-range cross-peaks in NOESY spectra, schematically represented in Figure 5.

The information from NOE's, amide exchange, chemical shifts, and coupling constants allows a qualitative description of aspects of the polypeptide structure to be developed. It is immediately apparent, for example, that there is no evidence for the presence of helical elements within the sequence. This conclusion is based on the strong intensities of $\alpha H_i - NH_{i+1}$ cross-peaks combined with only moderate intensity of NH−NH connectivities, the large values for $^3J_{HN\alpha}$, the lack of substantial stretches of $i,i+3$ NOE connectivities, and other diagnostic medium-range helical NOE indicators. By contrast, there is good evidence for the presence of β-sheet and turn motifs within the structure.

An antiparallel β-sheet linking strands 27−29 and 5−7, with the connecting turn formed by residues 1−4, is implied by the NOE data summarized in Figure 6. The long-range αH−αH NOE connectivities are diagnostic of antiparallel β-sheet structures, as are the amide exchange data that suggest the existence of four hydrogen bonds between residues 28 and 6 and 1 and 4, with amide protons for T28,

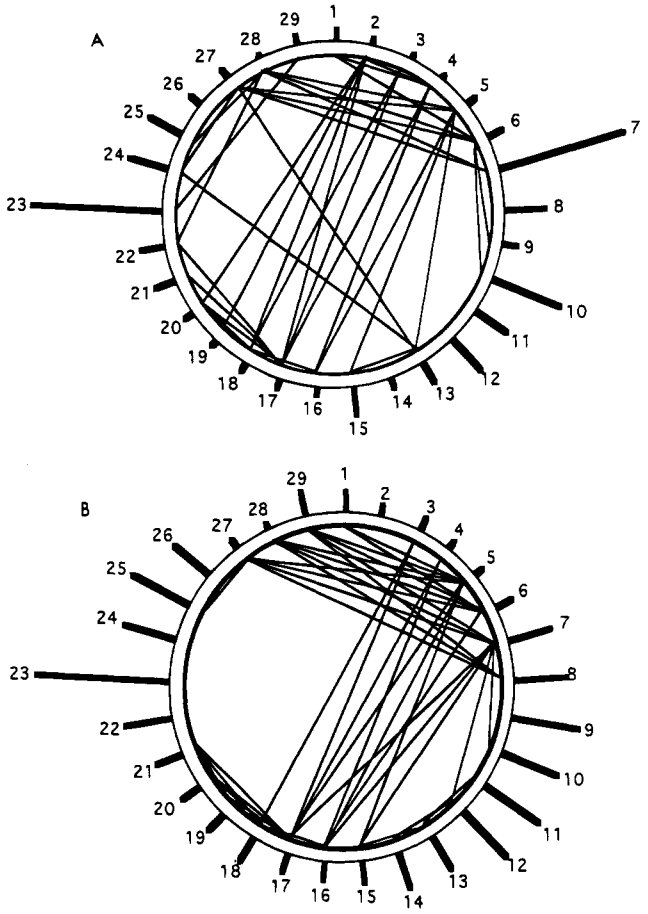

FIGURE 5: Spatial distribution of long-range distance restraints used in the structure determination (lines connecting residue numbers) and mean RMS coordinate differences per residue in structures calculated without disulfide bonds (external radiating thick lines): (A) restraints involving at least one component from a side chain; (B) restraints involving only αH and/or NH protons. RMS coordinate differences per residue were calculated using backbone non-hydrogen atoms only.

C29, V4, and T6 being slowly exchanging. This region of the molecule may thus be described as a β-hairpin. A third strand of the sheet links with the stretch from 3 to 7 and comprises residues 10−17, with a β-bulge occluding residues 13 and 14 from regular hydrogen bonding interactions. Some *i,i*+2 connectivities near residues 13 and 14 confirm a deviation from extended β structure in this region, as does the lack of slowly exchanging amide protons here.

Additional turns are centered on residues 8−9, 18−19, and 25−26, based on observed short-range NOE's and slowly exchanging amides. These deductions on the positions of turns are all consistent with the primary structure of the peptide, as the residues at the central positions, including glycine, proline, and asparagine, are commonly associated with turns in proteins.

In proteins with extensive regions of classical secondary structure, chemical shifts of the backbone α protons are often systematically perturbed compared with random coil shifts (Wishart et al., 1992). Plots of secondary shifts for the αH protons of kalata B1 versus residue position confirm the absence of helical regions (i.e., no extended regions of upfield shifts are observed) and the presence of several β-strands (demonstrated by downfield shifts for residues 4−7, 9−12, 15−17, 19−21, and 26−28). Some interesting observations were also made from chemical shifts of other protons. For example, there is a significant upfield deviation from random coil values for the shifts of Pro3. One of the β protons resonates at −0.25 ppm, a shift of more than 2 ppm from the random coil value. This deviation is attributed to ring current effects from the adjacent tryptophan residue. Other notable effects include significant downfield chemical shifts for the NH protons of T6 and T28 and an upfield shift for the NH of E15. The T6 and T28 residues are hydrogen-bonded to each other across two strands of β-sheet (Figure 6), the large downfield shifts suggesting a particularly strong pair of hydrogen bonds. The upfield shift for the NH of E15 supports the above interpretation of a β-bulge in the third strand of β-sheet as, in the absence of such a distortion, the E15 NH proton would likely be hydrogen-bonded to the carbonyl of C5. It would then be expected to be both downfield-shifted and slowly exchanging, neither of which occurs.

Three-Dimensional Structure Determination. The determination of protein structures by NMR normally utilizes a prior knowledge of both the primary sequence and disulfide connectivity. In the current study the latter was not available; however, because of the high quality of the recorded NOESY spectra combined with a large number of NOE constraints, in particular longer range constraints, it was thought feasible to determine the structure in the absence of disulfide connectivities and, indeed, to use the NMR data to establish these connectivities.

For a protein containing six cysteine residues, there are theoretically 15 possible ways of connecting them in pairs, with only one combination representing the native protein state. For kalata, the 15 possible connectivities are indicated in Table 2. Two approaches were used to establish whether the NOE data were sufficient to define a unique solution for the connectivity pattern and protein structure. In the first, a family of structures was calculated on the basis of the NOE constraints without any assumption of the disulfide connectivity; cysteine residues were not explicitly bonded. The resultant structures were examined to determine if the calculated positions of the sulfur atoms suggested that one particular set of disulfide connecitivities was more likely than other, theoretically possible, sets. This approach was recently applied in a study of the snake toxin, echistatin (Cooke et al., 1992). In the second approach, a separate family of structures (50 per set) was calculated for each of the 15 possible disulfide-bonded molecules. The resultant families of structures were compared to see if one was favored over the others.

For both approaches, the structure calculations were done using two computational protocols: simulated annealing based on random starting structures and a hybrid distance geometry/simulated annealing (DG/SA) method. Both protocols are described in the Materials and Methods section. The former was computationally more expensive, and therefore only 20 structures per set were calculated, compared with 50 per set for the DG/SA protocol, but it was utilized to check that no sampling bias were present in the protocol involving a distance geometry stage. It was found that the results were very similar for both methods, and in the following discussion only the results from the DG/SA calculations are described in detail.

A total of 459 distance restraints was used for the final structure determinations, and a summary of their distribution is given in Figures 4 and 5. An additional 20 restraints were

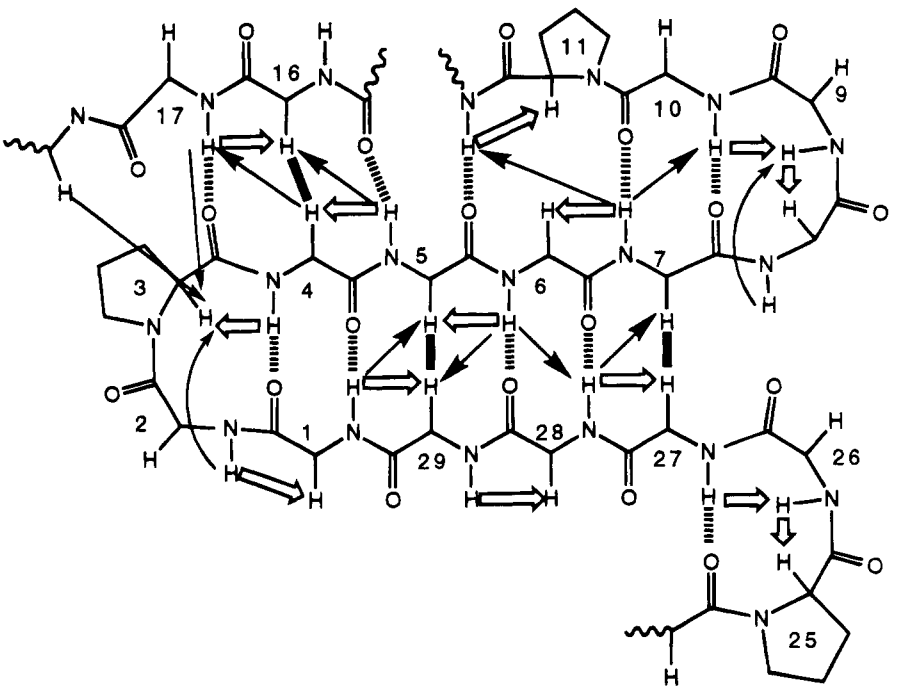

FIGURE 6: Secondary structural elements of kalata B1 deduced from a qualitative interpretation of NOE and slow-exchange amide data. The peptide backbone is labeled at the α-carbons with the residue number. Thick black lines represent cross-sheet αH−αH NOE's; thin black arrows represent NH_i−NH_j and NH_i−αH_j NOE's; thick white arrows represent sequential NH−αH NOE's; dashed lines show hydrogen bonds to slowly exchanging amide protons.

Table 2: Possible Disulfide Connectivities and RMSD of Disulfide Bonds

set	disulfide connectivity			RMSD[a]	N_{min}[b]
1	5−29	13−27	17−22	3.11	3
2	5−17	13−27	22−29	2.66	15
3	5−22	13−27	17−29	2.64	14
4	5−13	17−29	22−27	3.20	2
5	5−13	17−27	22−29	4.46	0
6	5−13	17−22	27−29	4.61	0
7	5−17	13−22	27−29	5.33	0
8	5−22	13−17	27−29	5.67	0
9	5−27	13−17	22−29	4.52	0
10	5−17	13−29	22−27	5.10	0
11	5−22	13−29	17−27	5.97	0
12	5−27	13−22	17−29	4.10	0
13	5−27	13−29	17−22	5.05	0
14	5−29	13−22	17−27	5.43	0
15	5−29	13−17	22−27	4.85	0

[a] Root mean square deviation in angstroms from the ideal S−S distance of 2.02 Å, summed for the three disulfide bonds in the indicated set. [b] Number of structures in which the given disulfide set had the lowest RMSD.

used to define 10 hydrogen bonds determined on the basis of slow amide proton exchange and preliminary structure refinements. These hydrogen bonds are illustrated in Figure 6. In cases where disulfide bonding was included, a further three distance restraints were used to position the sulfur atoms close to the correct bonding distance in the early stages of the simulated annealing calculations before they were formally bonded in the cooling stage. The S−S bond-included structures are referred to as sets 1−15 and are defined by the disulfide bonding patterns shown in Table 2. Structures calculated without disulfide bonding are referred to as no-SS. No dihedral angle constraints were included in the calculations.

(a) Refinement and Analysis of Structures with No Disulfide Bonds. After some preliminary structure calculations to determine the positions of hydrogen bonds, 50 structures were calculated using the DG/SA protocol. Sixteen of these had total energies more than three standard deviations above the lowest energy structure and were rejected. The remaining 34 structures all converged to a single global fold and exhibited a mean RMS backbone coordinate difference of 0.85 Å (SD = 0.24, min = 0.33, max = 1.57 Å). The residue-by-residue distribution of RMS deviations is illustrated in Figure 5, together with a representation of the nonsequential NOE's used in deriving the structures. Overall, the global fold is very well defined with two slightly disordered regions occurring near residues 23−25 and 7−12. The structures agree closely with earlier predictions with regard to elements of secondary structure.

Analysis of these non-disulfide-bridged structures consisted of measuring the observed S−S distances for the different possible disulfide combinations. Table 2 shows the collected data for each disulfide set, including the combined RMS deviation of the S−S bonds from the ideal separation of 2.02 Å, and the number of structures in which a particular disulfide set had the minimum deivation. Set 3 has the lowest RMSD overall and the minimum deviation in 14 of the 34 individual structures; however, sets 1, 2, and 4 have similarly low values for the RMSD. Set 2 has the lowest scoring pattern for 15 out of the 34 structures, set 1 for three and set 4 for two. Table 3 shows the mean S−S distance for individual disulfide bonds, together with a ranking of which bonds are best defined. The three best defined S−S bonds are 13−27, 17−29, and 5−17, two of which occur in both set 2 and set 3. The simple conclusion from these data is that the correct disulfide connectivity is most likely to be either set 2 or set 3, but it is not possible to distinguish these at this stage.

(b) Refinement and Analysis of Structures with Disulfide Bonds. The object of calculating structures with explicitly defined S−S bonds was to see if some sets were incompatible

Table 3: Mean SS Distances (Å) in Non-SS-bonded Model

bond	mean distance[a]	order[b]
5−13	4.59	4
5−17	4.31	2/3
5−22	4.93	5
5−27	4.99	6
5−29	5.19	7
13−17	8.39	12
13−22	7.77	11
13−27	4.08	1
13−29	9.36	15
17−22	5.46	9
17−27	8.48	13
17−29	4.31	2/3
22−27	6.03	10
22−29	5.25	8
27−29	8.53	14

[a] Mean distance in angstroms between sulfur atoms of the indicated residues. [b] Rank order of mean distances.

with the experimental constraints. The first feature to be considered in this type of approach is one of structural convergence. Intuitively, it seemed reasonable that if the correct disulfide bonding pattern was used in conjunction with the experimental restraints, then there would be a high convergence, and conversely, if one tried to force an incorrect bonding pattern, then the convergence would be low. However, although convergence may be a good test of restraints, it was concluded that this approach was potentially fallible due to the unpredictable nature of the simulated annealing pathway. It was decided that a better approach to assessing the validity of a bonding pattern would be to eliminate the nonconverged structures and judge the rest according to restraint violation and potential energy criteria.

Fifty structures were calculated for each of the 15 possible disulfide bonding patterns. The level of convergence varied significantly between different sets. In preparation for a comparison between final structures, nonconverged structures were removed. Set 3 exhibited the least spread of total energies and was used as a standard by which nonconverged structures from other sets could be eliminated. Eight of the structures within set 3 had energies significantly higher than the remainder and had clearly not converged. After elimination of these highest energy structures, the standard deviation (SD) of total energies for the remaining structures was 16 kcal/mol. For each of the 15 sets, any structures having an energy greater than 3 × SD (i.e., 48 kcal/mol) above the minimum for that set were removed. A measure of the differing degrees of convergence of the various data sets can be obtained from the number of structures from the original 50 that did not meet the cutoff criterion. The best was set 1, with three structures removed, and the worst was set 11, with 37 of the structures not meeting the energy cutoff. Convergence information for all data sets is given in Table 4.

So that each data set was compared on a uniform basis, a fixed number of the remaining structures from each set was chosen for further analysis. As the number of structures meeting the cutoff criterion for the worst set was 13, this was chosen as the sample number. Thirteen structures chosen at random from each of the sets were used for all subsequent analyses. Figure 7 shows the total and NOE energies (a measure of the restraint violation) for the 13 structures in each of the 15 sets. Set 3 contains the structure with the lowest energy of all those calculated and has the lowest mean value of both total and NOE energies (Table 4). It is closely followed by sets 1, 2, and 4, and some individual structures within these sets have energies lower than some in set 3. This analysis was repeated using the 13 lowest energy structures meeting the cutoff criterion from each set, and the same result was obtained (i.e., set 3 had

Table 4: Convergence, Energy, and Geometric Analyses of SS-Bonded Sets

					RMSD[e] (Å) (with no SS)		RMSD[f] (Å) (pairwise)	
set	N_r[a]	E_{min}[b] (kcal/mol)	E_{av}[c] (kcal/mol)	$E_{av/min}$[d] (kcal/mol)	bb	all	bb	all
1	3	154	180	161	1.08	1.81	1.01	1.62
2	16	155	176	154	1.25	1.95	1.06	1.73
3	10	136	155	138	1.10	1.72	0.84	1.44
4	16	156	174	151	1.18	1.83	0.89	1.53
5	13	205	225	218	1.75	2.41	1.35	1.98
6	13	187	203	178	0.97	1.68	0.80	1.43
7	15	205	223	213	1.70	2.37	1.07	1.61
8	15	208	225	206	2.01	2.87	0.97	1.48
9	11	192	215	183	1.82	2.57	1.13	1.71
10	22	217	237	230	1.57	2.24	1.03	1.61
11	37	272	293	276	2.46	3.02	0.76	1.34
12	11	165	189	166	1.70	2.33	0.84	1.46
13	23	222	246	225	1.42	2.09	1.22	1.84
14	33	255	280	261	2.05	2.65	1.25	1.80
15	12	194	210	195	2.01	2.81	0.99	1.55

[a] N_r = number of rejected structures from each set of 50 refined structures. [b] E_{min} = lowest total energy found among the final 13 refined structures. [c] E_{av} = mean total energy of each of the 13 refined structures. [d] $E_{av/min}$ = total energy of minimized average refined structures. [e] RMSD of 13 structures/set *vs* average structure from non-SS set. [f] RMSD for all pairwise superimpositions of 13 structures in each set: bb, backbone atoms only; all, all atoms except hydrogen atoms.

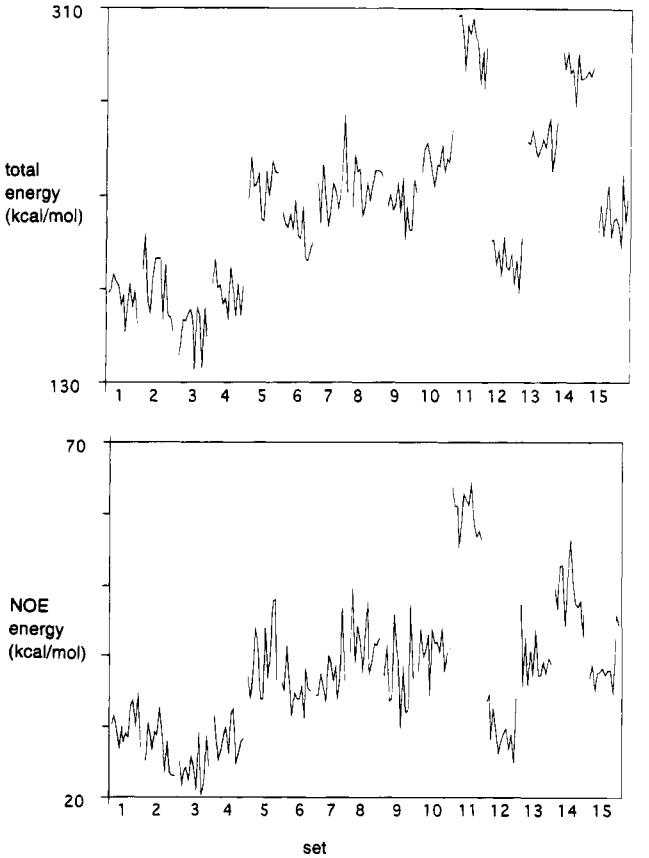

FIGURE 7: Plots of (a, top) total and (b, bottom) NOE energies for the 13 lowest energy structures (from a set of 50 calculated) for each of the 15 possible disulfide-bonded sets.

FIGURE 8: Calculated structures for each of the 15 possible disulfide connectivities (referred to as S1−S15). The global fold is represented by a solid ribbon corresponding to the average of the 13 lowest energy structures per set. The sulfur atoms are shown using a space-filling representation. (The break in the ribbon is due to a limitation in the display software, which does not cope with cyclic peptides.)

the lowest mean energy and included the lowest energy individual structure).

The geometries of the 15 sets are illustrated in Figure 8. In all cases except sets 11 and 14, the structures adopt approximately the same global fold. The fold is the same as that obtained for the calculations in which no disulfide pairing was imposed. The result suggests that global geometry alone cannot be used in this case to filter unlikely bonding patterns.

Table 4 shows that there is a rough correlation between convergence and energy, the highest energy sets (11 and 14) having poorer convergence than lower energy sets, although the correlation is not sufficiently precise to allow convergence alone to be used as a marker for the correct structure.

Table 4 shows the RMSD values for the 13 structures in each set paired with the average structure from the no-SS set. The best match between structures calculated with and without disulfide bonds is for set 6 followed by set 3. Again, however, sets 1, 2, and 4 are not significantly different.

Pairwise RMSD values over all combinations of the 13 structures within each set are given in Table 4. Interestingly, the lowest values are obtained for set 11, the set with the highest energy (Table 4) and clearly distorted global fold (Figure 8). The fact that set 11, a highly improbable structure based on all energy and convergence criteria, yields the best RMSD value of all sets serves to illustrate the need to distinguish the *precision* of a set of structures from their *accuracy* (Jardetzky et al., 1991). It would appear that, because of the significant strain associated with this structure, and its high energy, it possesses a rather steep energy minimum. While few structures converge to this local minimum, those that do are, of necessity, very well defined (i.e., convergent).

On the basis of the various criteria described above, it appears reasonable to conclude that set 3 represents the correct disulfide pairing in kalata B1. While sets 1, 2, and 4 cannot be eliminated from consideration, they do, in any case, possess the same global fold.

DISCUSSION

There are two interrelated aspects of this study that require discussion. The first involves a description of the structure of kalata B1 and its implications for understanding its biological activity, and the second relates to the methods developed here for establishing disulfide connectivity from NMR data and their possible application to other systems. As none of the proteases tested (including trypsin, chymotrypsin, pepsin, thermolysin, and the protease from *Staphylococcus aureus* V8) degrades native kalata B1, it was difficult to obtain information on the disulfide pairing by sequence analysis.

The structure of kalata consists of a compact sulfur core with the backbone fold derived from the elongated peptide cycle folded back onto itself and braced with disulfide pairs across diagonally opposed strands. Residues 27−7 form a β-hairpin with a type I β-turn centered at residues 2−3. Parallel to and below this hairpin are two extended strands involving residues 13−24, with the strands joined by a type I β-turn centered at residues 18−19. One of these strands forms a distorted third strand of β-sheet in combination with the hairpin, the distortion producing a bulge in the sheet structure near the terminus of one of the disulfide linkages (Cys13). This small section of β-sheet displays the characteristic right-handed twist often encountered in proteins (Chou et al., 1983; Chothia, 1973).

The turn at residues 18−19 is located directly below the β-turn at residues 2−3. This results in a number of residues, including proline, glycine, valine, and tryptophan, being in close proximity and forming an exposed surface patch on the molecule. The turn centered on residues 25−26 is of type II. A disordered loop involving residues 8−13 sits slightly apart from the core of the structure. Figure 9 shows a stereoview of kalata B1 in which the relative disposition of the β-turns at residues 2−3 and 18−19 is illustrated. In

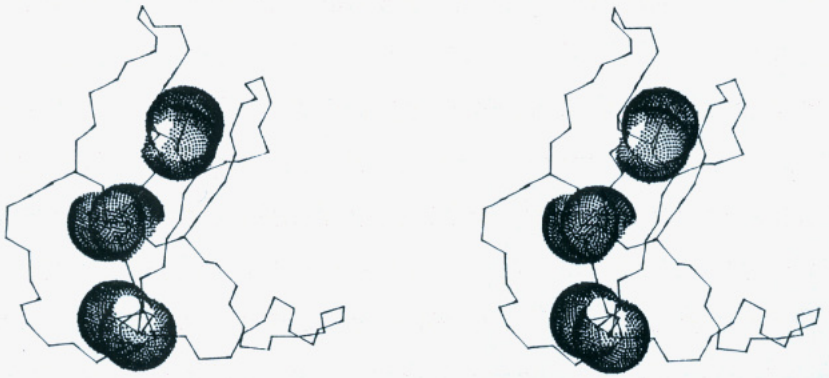

FIGURE 9: Stereoview illustrating the global fold of kalata B1. The structure is the lowest energy structure from set 3. The sulfur atoms from the cysteine residues are shown in space-filling form to illustrate the relative proximity of the three disulfide bonds: 17−29 (upper), 5−22 (middle), and 13−27 (lower). The relative proximity of the β-turns at residues 2−3 and 18−19 is also apparent in the upper part of the view. The loop corresponding to residues 8−13 is apparent at the lower right of the figure.

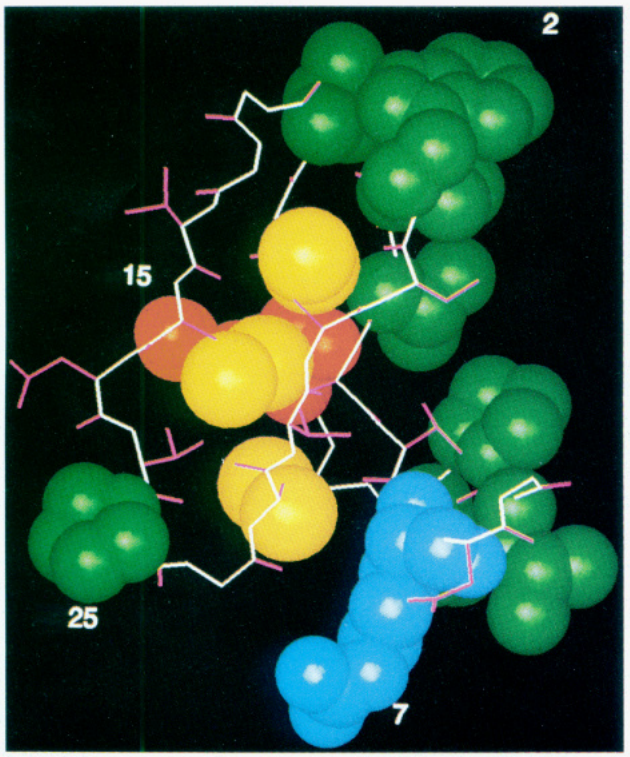

FIGURE 10: Calculated average structure of kalata B1 in which the hydrophobic residues are represented in space-filling mode to illustrate their concentration on one face of the molecule. Hydrophobic residues are colored green and sulfur atoms yellow. The backbone atoms are in white, and nonhydrophobic side chains are colored mauve. The two charged residues are represented in space-filling mode: Arg7 (blue) and Glu15 (red).

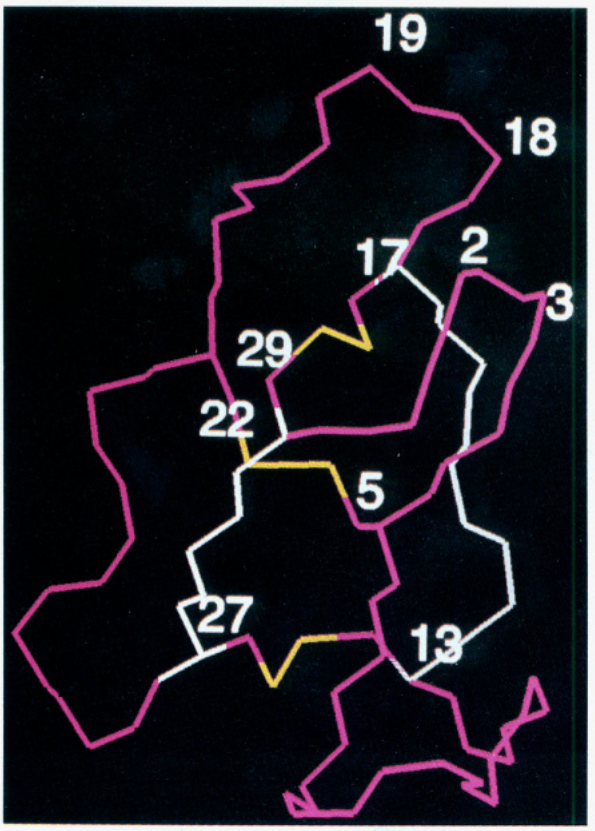

FIGURE 11: Structure illustrating the positions of proposed disulfide bonds (colored yellow) in kalata B1 (set 3). Note that the 5−22 disulfide bond passes through the loop formed by the peptide fragments (colored white) connected by the other two disulfide bonds.

this view the sulfur atoms from the cysteine residues are shown in space-filling form.

The structure derived for kalata is remarkably compact and may present a well-defined and highly characteristic surface to a receptor site. Figure 10 shows a space-filling representation of the structure which highlights the cysteine and hydrophobic residues. Most of the hydrophobic residues are concentrated along one face of the molecule, which may thus potentially be a surface that facilitates short-range van der Waals bonding interactions when the molecule is docked at a receptor site. The two charged residues, Arg7 and Glu15, are on opposite sides of this surface and could provide the necessary driving force for initial recognition and binding. No structure−activity data are available for analogues of this peptide, but it is interesting to speculate on a possible role for the loop from residues 8−13. As this apparently resides furthest from the core of the protein, it may have a degree of flexibility important in adapting the molecule to binding sites. As the basic shape of the rest of the molecule would likely remain unaffected by excision of this loop, the synthesis of a truncated analogue in which residues 6 and 14 are joined would be of assistance in establishing the functional role of the loop.

The three cysteine bonds in kalata B1 are assembled in a very tight central core; such an arrangement is not uncommon for multiple disulfide bonds. However, it is of particular interest to note that one of the disulfide bonds, 5−22, is threaded through the embedded loop formed by the two other

disulfides (which link the peptide fragments 13−17 and 27−29); i.e., a disulfide-linked eight amino acid cyclic structure has a third disulfide bond threaded through its center. This is illustrated in Figure 11, in which the relative geometry of the three disulfide bonds is shown.

Knotted topologies have been described for other small disulfide-containing proteins, most notably in trypsin inhibitors from the squash family (Holak et al., 1989; Heitz et al., 1989; Le Nguyen et al., 1990; Nielsen et al., 1994) and in a carboxypeptidase inhibitor (Rees & Lipscomb, 1980). It would appear that the knotted topology derived here for kalata represents a particularly stable arrangement, demonstrated by the exceptional thermal and chemical stability of the peptide. Similar intertwined disulfide linkages have also been found in other proteins, including nerve growth factor (NGF) (McDonald et al., 1991), transforming growth factor β2 (TGFβ2) (Daopin et al., 1992; Schlunegger & Grütter, 1992), and platelet-derived growth factor BB (PDGF-BB) (Oefner et al., 1992). These examples also involve a region of β-sheet near the intertwined disulfides, and their common structural motif has been dubbed the "cystine knot" (McDonald & Hendrickson, 1993). In NGF the third disulfide penetrates a 14-membered cystine ring, but in PDGF-BB and TGFβ2, an eight-membered ring is involved, as in kalata B1. It is thought that this represents the smallest ring through which the third disulfide bond may thread (Daopin et al., 1992).

It is of interest to compare this disulfide arrangement for kalata B1 with other topological possibilities. Benham and Jafri (1993) have recently reported on the general features of disulfide topologies in proteins, but the cyclic peptide backbone of kalata B1 introduces additional complexity. It should be noted that, for the sets of disulfide connectivities identified as likely, only one topology was observed in the calculated structures for each set. It is possible to envisage a number of topological isomers for each set, although in the current case these alternative topologies are excluded by the experimental restraints. Such topological isomers may, however, occur in other protein structures. It is also of interest to note that set 3 is the only connectivity pattern in which there is not at least one "non-knotted" topology.

In this study, the disulfide pattern of a polypeptide has been proposed on the basis of an extensive series of structure calculations of all possible alternatives. In the absence of independent chemical data defining the disulfide connectivity pattern of a given protein, other approaches to deriving this information might include deduction from NOE patterns between cysteines or by analogy with homologous proteins. The approach of using a qualitative examination of NOE cross-peaks for pairs of cysteine residues is not viable for kalata B1. For example, the disulfide bond that is apparently the best defined (as deduced from the structural data discussed earlier) is 13−27, and while there are NOE's between these residues, residue 13 also exhibits NOE's to another cysteine (Cys5). The next most probable connectivity (17−29), judging from the structural data, has no side-chain−side-chain NOE's linking the two residues involved. This contrasts with observations recently made from ^{1}H NMR spectra of iberiotoxin, a 37 amino acid scorpion toxin containing three disulfide bridges (Johnson & Sugg, 1992). As in the current study, it had not proved possible to chemically determine the linkages prior to NMR investigation. In that study, apparently unambiguous NOE's were detected between paired cysteines for two of the three disulfide bonds. Once two bonds are defined, the third follows by default. The connectivities suggested in this way were consistent with structures calculated without forcing a particular connectivity pattern and with known connectivities from homologous toxins (Johnson & Sugg, 1992).

CONCLUSION

The global fold of kalata B1 and the positions of many of the side chains have been defined in the absence of disulfide bond information. The peptide has been shown to be made up of largely β-strand, connected by tight turns, surrounding a sulfur core. One of the most striking features of the determined kalata B1 structure is the relatively large hydrophobic surface presented on one face. The peptide is compact and highly structured, partly as a consequence of the cross-braced disulfide core but also due to a large number of hydrogen bonds holding parts of the β-strand into antiparallel sheet. The two charged residues are found at diametrically opposed positions, away from the hydrophobic patch. Of the 15 possible disulfide bonding patterns, four are classed as possible (sets 1, 2, 3, and 4) and one as most probable (set 3). Due to the small size of kalata B1, it was computationally feasible to refine all possible combinations of disulfide bridges. The approach used in the current study of using both a non-sulfur-bonded refinement and one in which all possible bonding combinations are used explicitly was computationally demanding and would not be practical in a situation involving more than three disulfide bonds. By exhaustive examination of a molecule like kalata B1, we have shown that a general technique for determining disulfide connectivities by NMR spectroscopy could involve a first stage of calculation using nonbonded cysteines, followed by explicit calculations on only those bond options indicated as likely.

ACKNOWLEDGMENT

We are grateful to Dr. Robin Aplin for mass spectrometry analysis and to Dr. Paul Barlow for helpful discussions. D.J.C. thanks the Victorian College of Pharmacy for sabbatical leave, during which this work was undertaken.

REFERENCES

Austen, B. M., & Smith, E. L. (1976) *Biochem. Biophys. Res. Commun. 72*, 411−417.
Bax, A. (1988) *Methods Enzymol. 176*, 151−168.
Bax, A., & Davis, D. G. (1985) *J. Magn. Reson. 65*, 355−366.
Benham, C., & Jafri, M. S. (1993) *Protein Sci. 2*, 41−54.
Bodenhausen, G., Vold, R. L., & Vold, R. R. (1980) *J. Magn. Reson. 37*, 93−106.
Bornstein, P. (1970) *Biochemistry 9*, 2408−2421.
Braunschweiler, L. R., & Ernst, R. R. (1983) *J. Magn. Reson. 53*, 521−528.
Brooks, B. R., Bruccoleri, R. E., Olafson, B. D., Sates, D. J., Swaminathan, S., & Karplus, M. (1983) *J. Comput. Chem. 4*, 187−217.
Brünger, A. T. (1992) *X-PLOR Manual (Version 3.0)*, Yale University Press, New Haven, CT.
Chothia, C. (1973) *J. Mol. Biol. 75*, 295−302.
Chou, K.-C., Nimely, G., & Scheraga, H. A. (1983) *J. Mol. Biol. 168*, 389−407.
Cooke, R. M., Carter, R. G., Murray-Rust, M., Hartshorn, M. J., Herzyk, P., & Hubbard, R. E. (1992) *Protein Eng. 5*, 473−477.

Daopin, S., Pier, K. A., Ogawa, Y., & Davies, D. (1992) *Science 257*, 369−373.
Davis, D. G., & Bax, A. (1985) *J. Am. Chem. Soc. 107*, 2821−2822.
Fontana, A. (1972) *Methods Enzymol. 25*, 419−423.
Gran, L. (1970) *Medd. Nor. Farm. Selsk. 12*, 173−180.
Gran, L. (1973a) *Lloydia 36*, 174−178, 207−208.
Gran, L. (1973b) *Acta Pharmacol. Toxicol. 33*, 400−408.
Heitz, A., Chiche, L., Le Nguyen, D., & Castro, B. (1989) *Biochemistry 28*, 2392−2398.
Hirs, C. H. W. (1956) *J. Biol. Chem. 219*, 611−621.
Holak, T., Gondol, D., Otlewski, J., & Wilusz, T. (1989) *J. Mol. Biol. 210*, 635−648.
Jardetzky, O. (1991) in *Computational Aspects of the Study of Biological Macro-molecules by Nuclear Magnetic Resonance Spectroscopy* (Hoch, J. C., Poulsen, F. M., & Redfield, C., Eds.) Plenum Press, New York.
Jeener, J., Meier, B. H., Bachmann, P., & Ernst, R. R. (1979) *J. Chem. Phys. 71*, 4546−4553.
Johnson, B. A., & Sugg, E. E. (1992) *Biochemistry 31*, 8151−8159.
Klaus, W., Broger, C., Gerber, P., & Senn, H. (1993) *J. Mol. Biol. 232*, 897−906.
Le Nguyen, D., Heitz, D., Chiche, L., Castro, B., Boigegrain, R. A., Favel, A., & Coletti-Previe, M. A. (1990) *Biochimie 72*, 431−435.
Macura, C., Huang, Y., Suter, D., & Ernst, R. R. (1981) *J. Magn. Reson. 43*, 259−281.
Marion, D., & Wüthrich, K. (1983) *Biochem. Biophys. Res. Commun. 113*, 967−974.
Marion, D., & Bax, A. (1988) *J. Magn. Reson. 79*, 352−356.
McDonald, N. Q., & Hendrickson, W. A. (1993) *Cell 73*, 421−424.
McDonald, N. Q., Lapatto, R., Murray-Rust, J., Gunning, J., Wlodawer, A., & Blundell, T. L. (1991) *Nature 354*, 411−414.
Nielsen, K. J., Alewood, D., Andrews, J., Kent, S. H. B., & Craik, D. J. (1994) *Protein Sci. 3*, 291−302.
Nilges, M. (1990) in *X-PLOR Manual (Version 2.1)* (Brünger, A. T., Ed.) pp 256−263, Yale University Press, New Haven, CT.
Nilges, M., Clore, G. M., & Gronenborn, A. M. (1988) *FEBS Lett. 239*, 129−136.
Oefner, C., D'Arcy, A., Winkler, F. K., Eggiman, B., & Hosang, M. (1992) *EMBO J. 11*, 3921−3926.
Plateau, P., & Gueron, M. (1982) *J. Am. Chem. Soc. 104*, 7310−7311.
Rance, M., Sørensen, O. W., Bodenhausen, G., Wagner, G., Ernst, R. R., & Wüthrich, K. (1983) *Biochem. Biophys. Res. Commun. 117*, 479−485.
Redfield, A. G., & Kuntz, S. D. (1975) *J. Magn. Reson. 19*, 250−254.
Rees, D. C., & Lipscomb, W. N. (1980) *Proc. Natl. Acad. Sci. U.S.A. 77*, 4633−4637.
Saudek, V., Atkinson, R. A., & Pelton, J. T. (1991) *Biochemistry 30*, 7369−7362.
Schlunegger, M. P., & Grütter, M. G. (1992) *Nature 358*, 430−434.
Sletten, K., Natvig, J. B., Husby, G., & Juul, J. (1981) *Biochem. J. 195*, 561−572.
Wishart, D. S., Sykes, B. D., & Richards, F. M. (1992) *Biochemistry 31*, 1647−1651.

BI942115J